Journal of Molecular Modeling (2020) 26: 128
https://doi.org/10.1007/s00894-020-04388-3

ORIGINAL PAPER

Structural, electronic, and energetic investigations of acrolein adsorption on B_{36} borophene nanosheet: a dispersion-corrected DFT insight

Hamza Allal[1] · Youghourta Belhocine[2] · Seyfeddine Rahali[3] · Maamar Damous[2,4] · Nesrine Ammouchi[1]

Received: 8 March 2020 / Accepted: 22 April 2020 / Published online: 9 May 2020

Abstract

The adsorption of acrolein (AC) onto the surface of B_{36} borophene nanosheet was studied using dispersion-corrected density functional theory (DFT). The structural and electronic properties were scrutinized by several quantum chemical parameters such as HOMO–LUMO gap, condensed Fukui function, molecular electrostatic potential (ESP), and the density of states (DOS). The non-covalent interactions (NCI) were explored by combined reduced density gradient (RDG-NCI) and energy decomposition analysis (EDA) techniques. It was found that the adsorption of acrolein on both convex and concave surfaces of borophene is mainly governed by van der Waals interactions. Our calculations showed that the adsorption energy is strengthened and favored when multiple acrolein molecules adsorb on the edge sides of borophene through their terminal carbonyl oxygen atom. Furthermore, the calculated HOMO–LUMO energy gaps were significantly reduced upon adsorption affecting, therefore, the electrical conductance of borophene. These results should be useful in designing acrolein sensors.

Keywords Borophene · Sensor · Acrolein · Adsorption · DFT · Electronic properties

Introduction

The recent emergence of new two-dimensional (2D) materials opened up a diversity of new applications in the fields of environment, energy storage, electronics, and biomedical engineering [1–11]. The first two-dimensional material known as graphene was synthesized by Novoselov et al. in 2004 [12]. Since its discovery, graphene has been a focus of numerous theoretical and experimental studies [13–20].

Very recently, new post-graphene 2D materials such as stanene [21–24], germanene [25], bismuthene [26], and borophene [27–31] were discovered after being theoretically predicted. Particular attention is drawn to the borophene, an allotropic form of two-dimensional boron defined as boron sheet which has been synthesized by depositing vaporizing boron on silver Ag(111) substrate [27]; the miscellaneous bonding configurations adopted by boron nanosheets allow the borophene to exhibit a polymorphism and different crystal structures, consisting of combined hexagonal and triangular motifs, thus resulting in the following most common polymorphs denominated β_{12} and χ_3 and striped–borophenes [27, 28]. Diverse borophene allotropes could be obtained experimentally by controlling the synthesis conditions such as the nature of the substrate and its crystallographic orientation dependence [32].

New architectures based on 2D boron nanosheets have also been developed to enrich the class of borophene clusters [33–37]. Among them, the smallest borophene (B_{36}) cluster [38] having sixfold symmetry was experimentally evidenced and described as a highly stable flattened bowl-shaped boron

Electronic supplementary material The online version of this article (https://doi.org/10.1007/s00894-020-04388-3) contains supplementary material, which is available to authorized users.

✉ Hamza Allal
hamzaallal.univ@gmail.com

[1] Department of Technology, Faculty of Technology, 20 August 1955 University of Skikda, P.O. Box 26, El Hadaik Road, 21000 Skikda, Algeria

[2] Department of Petrochemical and Process Engineering, 20 August 1955 University of Skikda, P.O. Box 26, El Hadaik Road, 21000 Skikda, Algeria

[3] Department of Chemistry, College of Science & Arts at Al-Rass, Qassim University, P.O. 53, Buraydah, Saudi Arabia

[4] Unité de Recherche de Chimie de l'Environnement et Moléculaire Structurale, CHEMS, Université Constantine 1, 25000 Constantine, Algeria

cluster bearing a hexagonal vacancy at the center [39–41]. The latest reports show that borophene, with its both metallicity and lightweight properties [27], has an interesting potential for catalysis, hydrogen storage, and high capacity electrode [42–46]. Additionally, borophene is a promising chemical sensor material and could be used for making sensing devices for detecting toxic substances [47, 48].

Acrolein (AC) or 2-propenal is an organic compound and the simplest unsaturated three-carbon aldehyde; it is used mainly as a pesticide and as a precursor for producing acrylic acid. However, exposure to the acrolein vapor causes mucosal inflammation; it is highly toxic if inhaled and irritating to the skin, eyes, and upper respiratory tract even at low levels of concentrations; acrolein released from tobacco smoke is associated with respiratory toxicity [49]; it was also reported that acrolein could potentially be human carcinogenic [50].

Due to the importance of designing high sensitive devices capable of detecting acrolein, a number of computational investigations focused on the adsorption of acrolein on various adsorbent materials were carried out [51–58]. The ability of pristine and Al-doped graphenes to adsorb acrolein has been studied using DFT by Rastegar et al. [51]; their investigations confirmed the sensitivity of Al-doped graphene toward acrolein. Karami [52] reported a DFT study of acrolein adsorption on graphyne nanotube and revealed the potential of graphyne sheets for acrolein sensing applications. Pirillo et al. [55] explored theoretically the adsorption properties of acrolein on Pt(111); the authors indicated that the adsorption process is mainly due to the formation of C–Pt bonds.

Quantum chemical calculations may provide a tremendous insight regarding the adsorption process including the nature of involved interactions; it is worth noting that numerous 2D materials were predicted theoretically before being experimentally confirmed.

Herein, the plausibility of adsorption of acrolein on borophene B_{36} was assessed with dispersion-corrected density functional calculations; geometrical parameters and electronic structures, as well as the adsorption properties of the interacting systems, have been examined systematically.

Computational details

The geometries of all studied structures in this work were optimized using DFT-D3 methodology where dispersion correction with Becke–Johnson D3(BJ) and standard zero D3(0) damping functions are applied to account for the dispersion interactions. B3LYP-D3(BJ) [59–62], B97-D3(BJ) [60, 63], and M06-2X-D3(0) [59, 60, 64] levels of calculations were employed and combined with the def2-SVP [65–67] basis set in vacuum. These computations were carried out with ORCA program package [68] (version-4.2.0). For improving the computational efficiency procedure, the resolution of identity (RI) and chain of spheres exchange (COSX) approximations were applied [69–71]. A geometrical counterpoise correction (gCP) was incorporated to account for the basis set superposition error (BSSE) [72]. The frequency calculations were performed in order to confirm and verify the minima of all obtained stationary points. The visualization of the molecular orbitals was performed with the Avogadro software [73]. Analysis of weak intramolecular and intermolecular interactions between AC molecule and B_{36} nanosheet was carried out with the non-covalent interaction-reduced density gradient analysis approach (NCI-RDG) [74] using the Multiwfn software [75] and VMD visualization program [76]. The energy decomposition analysis (EDA) was determined with the GAMESS code [77] by the M06-2X [62] functional and 6-31G(d,p) basis set [78].

The adsorption energy is calculated according to the following expression [79–90]:

$$E_{ads} = \left(E\left[B_{36}(AC)_n\right] - E(B_{36}) - nE(AC)\right)/n \quad (1)$$

where $E[B_{36}(AC)n]$ corresponds to the total energy of the $B_{36}(AC)n$ complex, $E(B_{36})$ is the energy of the isolated B_{36} nanosheet, and $E(AC)$ is the energy of the isolated single AC molecule.

The change in the HOMO–LUMO gap $|\Delta E_g|$, as an indicator of the electronic sensitivity of the B_{36} toward the dissociative adsorption of AC molecule, is obtained by:

$$|\Delta E_g| = \left[\left(E_{g2} - E_{g1}\right)/E_{g1}\right] \times 100 \quad (2)$$

where E_{g1} and E_{g2} are, respectively, the values of E_g in the initial and the final states.

Results and discussion

Properties of B_{36} borophene

The optimized geometry of the B_{36} borophene nanosheet was determined by the following theoretical levels of calculations: B3LYP-D3(BJ)/def2-SVP, B97-D3(BJ)/def2-SVP, and M06-2X-D3(0)/def2-SVP. Our results are corroborated by the experimental data [38] and previous theoretical [79–86] studies, indicating that the B_{36} borophene is consisting of three different sizes of rings: internal (B_1–B_6), median (B_7–B_{18}), and external rings (B_{19}–B_{36}), as shown in Fig. 1. The B_{36} borophene bears a quasi-planar structure with a central hexagonal hole and exhibits a perfect hexagonal C_{6v} symmetry [48, 81]. The optimized structure at B97-D3(BJ)/def2-SVP predicts different B–B bond lengths ranging between 1.609 and 1.749 Å and close to the values calculated by Rostami and Soleymanabadi [80]. Frequency calculations were performed at the same level of theory for the reported structures without producing imaginary frequencies.

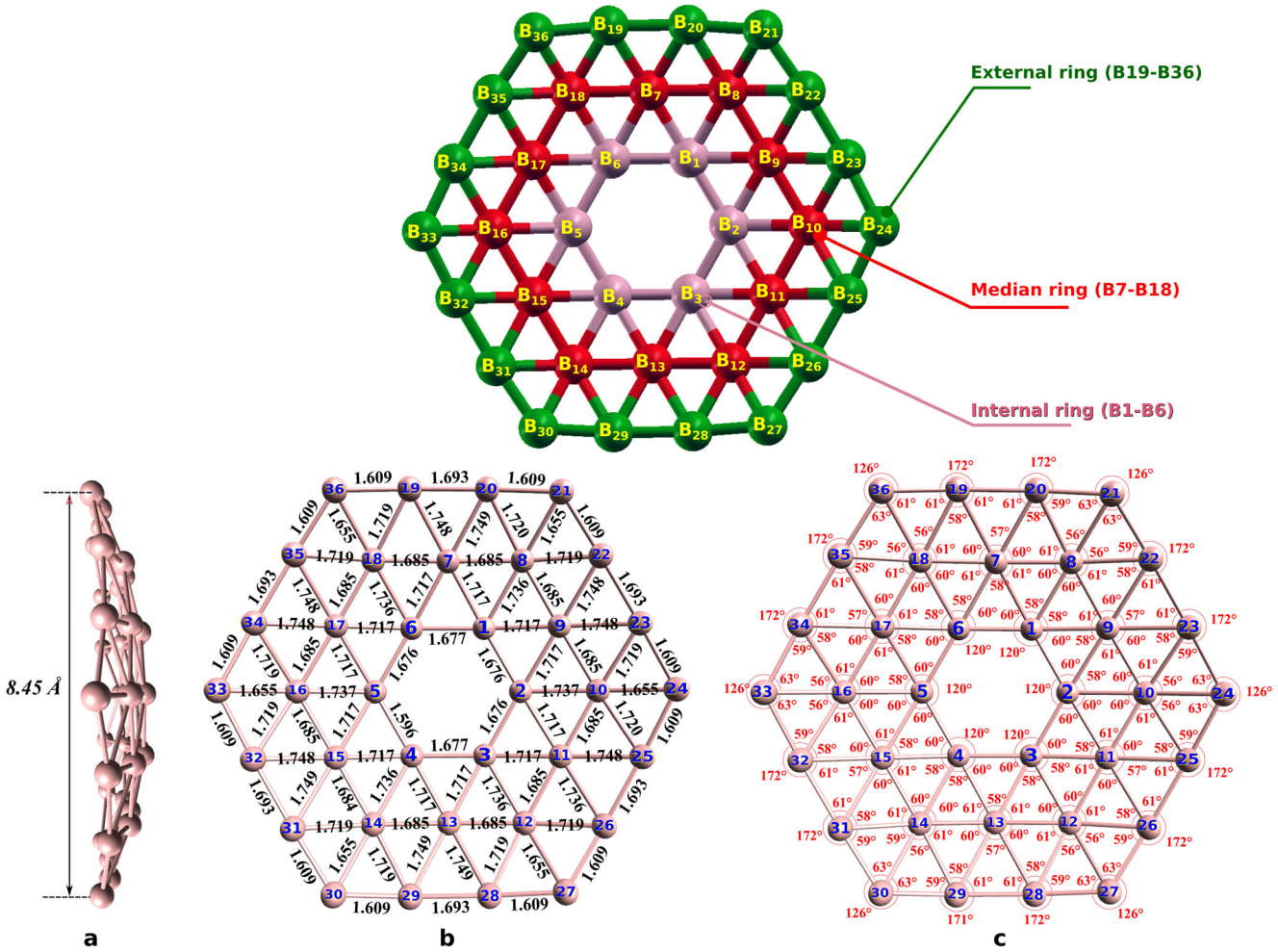

Fig. 1 Optimized geometry structure of the B_{36} nanosheet calculated at the B97-D3(BJ)/def2-SVP level. (A) Side view; (B), (C) top views; (B): with bond lengths (Å) and (C): with bond angles (°)

The calculated electronic parameters, such as the frontier molecular orbital energy (E_{HOMO}, E_{LUMO}) and HOMO–LUMO gap energy $|E_g|$, offer a valuable method for evaluating the reactivity and stability of such molecular systems [81–86], where smaller E_g (absolute values) indicates high reactivity, whereas larger values of $|E_g|$ show a greater stability [91, 92].

Based on the calculated values of $|E_g|$ (Table 1), it was found that the neutral B_{36} nanosheet is more reactive than cationic and anionic species, following the order: $B_{36} > B_{36}^{-} > B_{36}^{+}$. The larger HOMO–LUMO gaps predicted by M06-2X functional are due to its higher amount of exact Hartree-Fock (HF) exchange (54%). These results are in agreement with previous similar studies [93–95] which concluded that increasing HF exchange percentage in DFT functionals leads to the increase of HOMO–LUMO gap.

The condensed Fukui function (Fig. 2) and molecular electrostatic (ESP) potential (Fig. 3) were used as reactivity descriptors in assessment and prediction of the most reactive centers, especially nucleophilic and electrophilic sites.

In the literature [91–94, 96], it has been reported that the preferred center for electrophilic attack is the atom in the molecule where the value of f^- is the highest, while the site for nucleophilic attack is the atom in the molecule where the value of $f^+$is the highest.

The calculated values of the Fukui functions (f^+ and f^-) are illustrated in Fig. 2. The results predict that f_k^+ values are highest on the external rings of neutral B_{36} borophene, precisely on the corner sites (B_{21}, B_{24}, B_{27}, B_{30}, B_{33}, and B_{36} atoms), suggesting that these sites would be most favorable for nucleophilic attack. The most susceptible sites for electrophilic attacks are B_2, B_5, B_7, and B_{13} atoms, followed by atoms of the corner sites B_{21}, B_{24}, B_{27}, B_{30}, B_{33}, and B_{36}. This observation clearly establishes that the most reactive sites are those located at the corner sites of neutral B_{36}, susceptible to both nucleophilic and electrophilic attacks. These findings are supported by several studies [48, 82, 84] indicating that the edge boron atoms of neutral B_{36} borophene are more reactive than the inner atoms.

Table 1 The frontier molecular orbital energy (E_{HOMO} and E_{LUMO}) and HOMO–LUMO gap$|E_g|$, dipole moment (μ), and total energy (TE) in kcal mol^{-1} of B_{36}, B_{36}^{+}, and B_{36}^{-} nanosheets

Method		E_{HOMO} (eV)	E_{LUMO} (eV)	$\|E_g\|$ (eV)	μ (Debye)	TE (kcal mol^{-1})
B3LYP- D3(BJ)	B_{36}	− 5.73	− 3.85	1.88	2.43	− 560,365.94
	B_{36}^{-}	2.98	− 0.85	3.83	2.98	− 560,365.94
	B_{36}^{+}	1.93	− 6.99	8.92	1.93	− 559,738.43
B97-D3(BJ)	B_{36}	− 5.39	− 4.30	1.09	2.31	− 560,365.94
	B_{36}^{-}	2.79	− 1.30	4.09	2.79	− 560,365.94
	B_{36}^{+}	1.80	− 7.43	9.23	1.80	− 559,738.43
M06-2X-D3(0)	B_{36}	− 6.89	− 3.50	3.39	2.40	− 560,365.94
	B_{36}^{-}	2.94	− 0.50	3.44	2.94	− 560,365.94
	B_{36}^{+}	1.94	− 6.62	8.56	1.94	− 560,365.94

Figure 3 shows the ESP maps of the van der Waals surface of the optimized neutral B_{36}, in which the blue and red regions on the scale bar indicate respectively the lowest and highest ESP energy values. The surface local minima and maxima of ESP are represented respectively by cyan and orange spheres.

The inspection of the calculated ESP plots on the van der Waals surface revealed that the local minima of ESP surface are dispersed near the outer side of B_{36} (external ring "B_{19}–B_{36}"), with larger negative values (− 5.874 to − 5.907 kcal mol^{-1}); thus, they could act as reactive sites and also may favor the electrophilic reaction.

The positive ESP regions on the van der Waals surface with a large value (i.e., > 17 kcal mol^{-1}) are distributed in both convex and concave sides of B_{36} surface, in which their local maxima of ESP are significant but relatively larger on the concave side (21.618 to 21.653 kcal mol^{-1}) than convex side (17.451 to 17.546 kcal mol^{-1}). This interesting observation suggests that the concave side is chemically more reactive than the convex side.

Adsorption of single acrolein molecule on the B_{36} borophene

In order to find and examine the most stable adsorption geometries, several initial configurations of AC adsorption on the B_{36} borophene were investigated, taking into consideration the convex and concave shapes of the B_{36} borophene surface and various possible orientations of AC molecule. With this aim, we have explored various sites by placing the oxygen atom of the acrolein molecule on top of the boron atoms, and also by orienting the AC molecule both in perpendicular and parallel directions to the B_{36} borophene sheet, as shown in supplementary data (see Fig. S1).

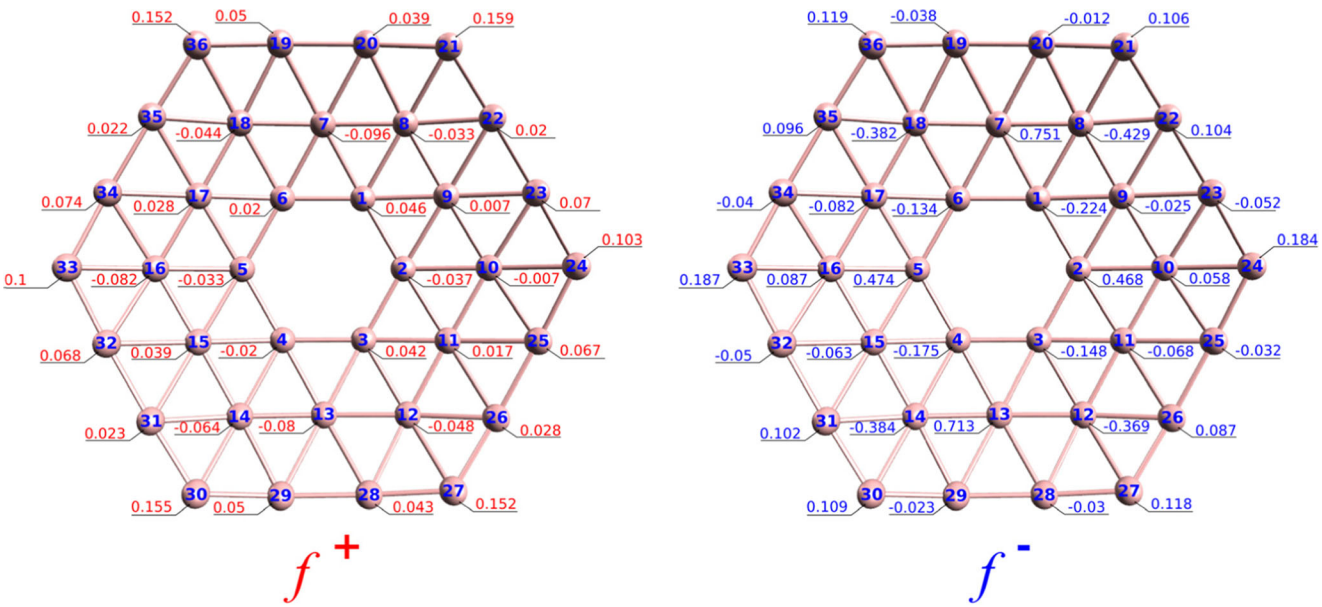

Fig. 2 The calculated Fukui functions of the B_{36} nanosheet; (left) nucleophilic attack $f^{+}$and (right) electrophilic attack f^{-}

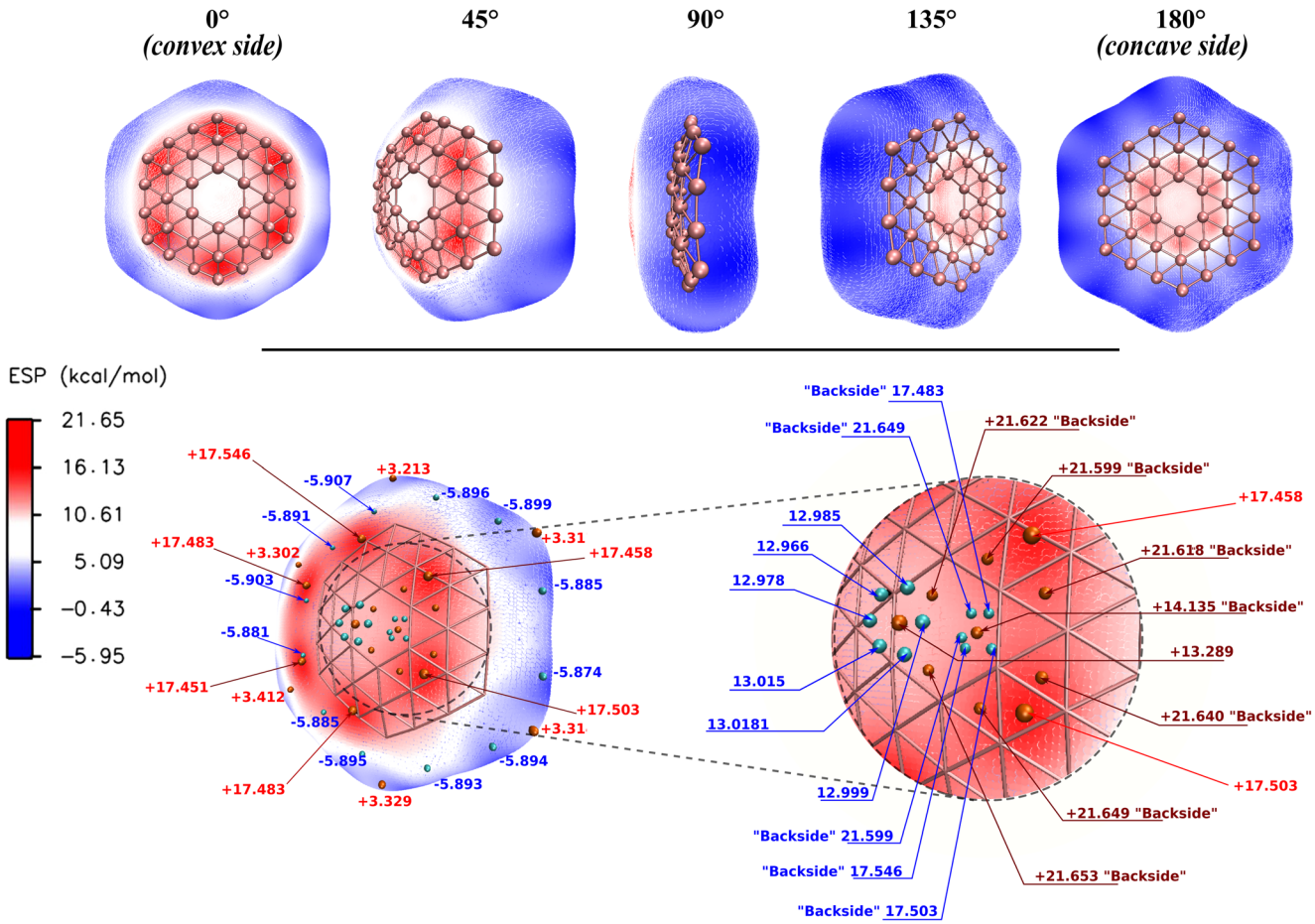

Fig. 3 The molecular electrostatic potential (ESP) surfaces of the B_{36} nanosheet; negative ESP regions are indicated in blue, and the positive regions in red

Different configurations for the adsorption of the acrolein on B_{36} borophene were considered in this study. However, only geometries with local minima obtained at the B97-D3(BJ)/def2-SVP level of theory were kept, in which the calculated adsorption energy was higher than − 0.99 kcal mol^{-1}, indicating that the adsorption is spontaneous and the process is exothermic. Three local minima are selected with an adsorption energy higher or equal to − 9.8 kcal mol^{-1}. Figure 4(B)–(D) show the optimized geometries of the three most stable configurations, and their associated frontier molecular orbital distributions (HOMO and LUMO).

The most stable formed complex is (B), in which the AC molecule is attached via the oxygen atom of its carbonyl group to the boron atom of corner (edge) site of B_{36} structure. The calculated adsorption energy is − 25.20 kcal mol^{-1}, and the newly formed bond length B–O was 1.466 Å. As shown in Table 2, the maximum change of $|\Delta E_g|$ has been observed in the edge configuration ($|\Delta E_g| = 67.10\%$), where both HOMO and LUMO levels were shifted respectively to higher and lower energies, thus resulting in the significant decrease of HOMO–LUMO gap.

From Table 2, it can be observed that the adsorption energies decrease in the following order: E_{ads} edge > E_{ads} concave > E_{ads} convex. The calculated density of states (DOS) for B_{36} nanosheet and its three complexes AC@B_{36} edge, AC@B_{36} concave, and AC@B_{36} convex is illustrated in Fig. 5. The results clearly reveal that the AC@B_{36} edge complex affects strongly the electronic properties of B_{36} borophene if compared with both AC@B_{36} concave and AC@B_{36} convex.

For C and D complexes (Fig. 4), the AC molecule is horizontally adsorbed on the concave and convex surfaces of B_{36} borophene with the adsorption energies of − 15.28 and − 9.60 kcal mol^{-1} respectively, indicating a weak interaction. This observation is obviously consistent with our previous ESP analysis (Fig. 3) which predicted that the concave side of B_{36} borophene is relatively more reactive than the convex side.

Furthermore, we introduced the non-covalent interaction (NCI) analysis based on the reduced density gradient (RDG) function, in order to analyze the intermolecular interactions and to distinguish the nature of the interactions between the AC molecule and B_{36} nanosheet. The RDG quantities are calculated by the following equation [93, 94, 96–100]:

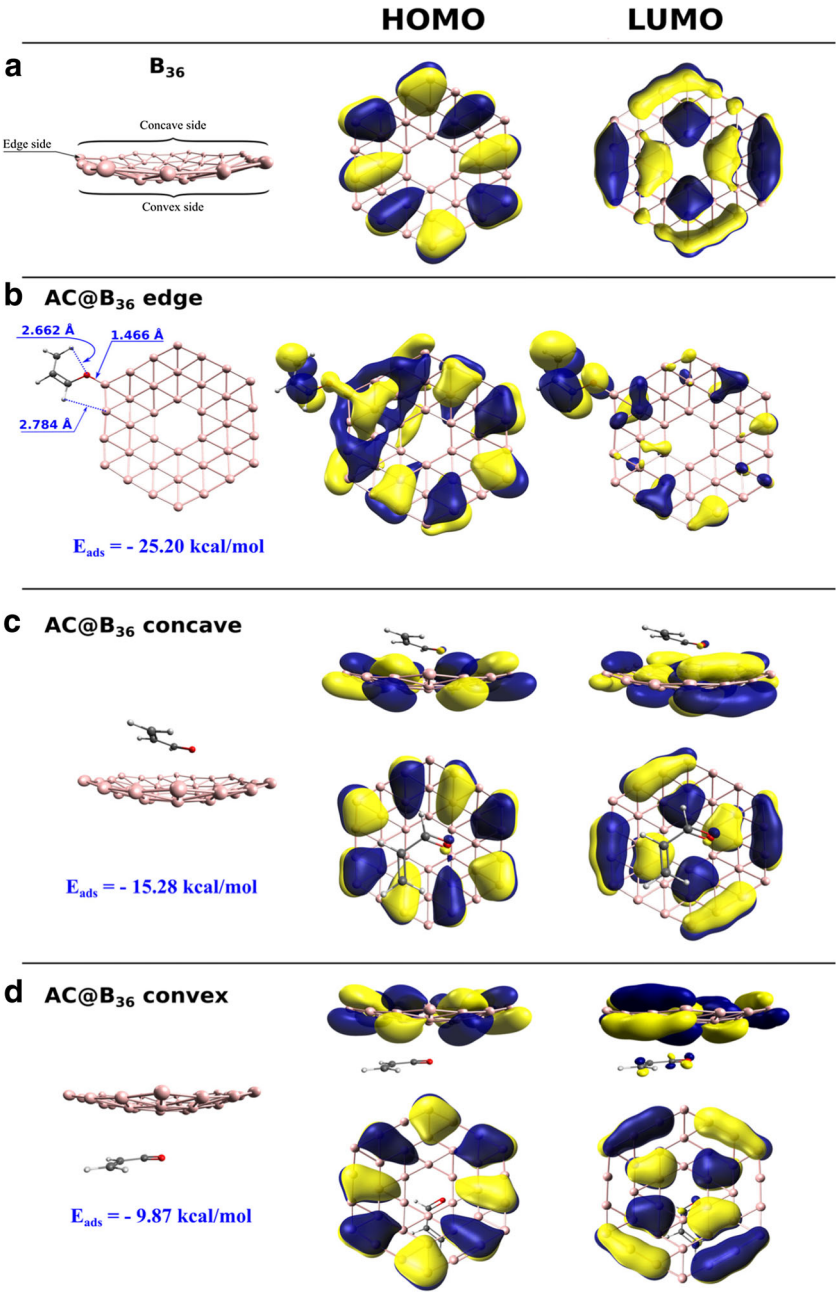

Fig. 4 The optimized geometries and frontier molecular orbital distributions HOMO and LUMO of (A) B_{36} nanosheet and the three most stable complexes: (B) AC@B_{36} edge, (C) AC@B_{36} concave, and (D) AC@B_{36} convex

Table 2 Adsorption energy (E_{ads}, kcal mol^{-1}), HOMO and LUMO energies (E_{HOMO} and E_{LUMO}, eV), HOMO–LUMO energy gap ($|E_g|$, eV), and the change of $|E_g|$ after the adsorption process ($|\Delta E_g|$) for studied B, C, and D complexes

Complex	E_{ads} kcal mol^{-1}			E_{HOMO} (eV)	E_{LUMO} (eV)	$\|E_g\|$ (eV)	$\|\Delta E_g\|$ (%)
	B3LYP-D3(BJ)	B97-D3(BJ)	M06-2X-D3(0)				
B_{36}	–	–	–	− 5.39	− 4.30	1.09	–
B (edge)	− 25.65	− 25.20	− 22.18	− 4.95	− 4.59	0.36	67.10
C (concave)	− 15.17	− 15.28	− 11.36	− 5.32	− 4.25	1.07	1.68
D (convex)	− 9.24	− 9.87	− 3.51	− 5.33	− 4.24	1.09	0.42

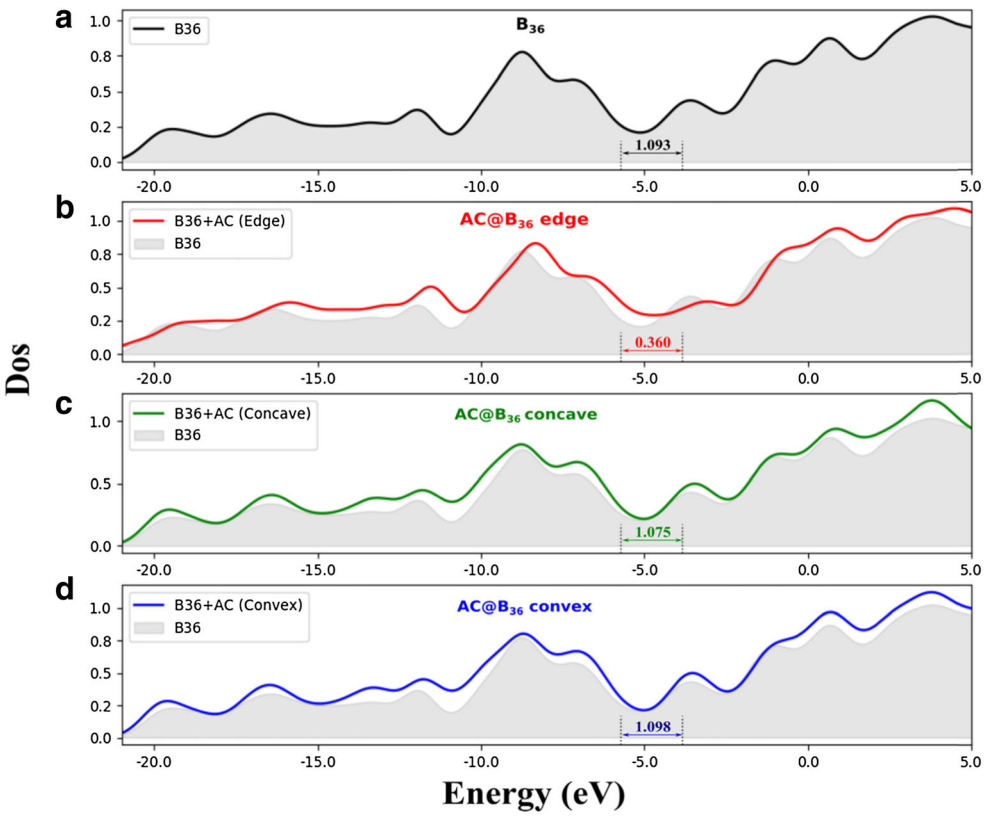

Fig. 5 The density of states (DOS) of (A) B_{36} nanosheet and the three most stable complexes: (B) AC@B_{36} edge, (C) AC@B_{36} concave, and (D) AC@B_{36} convex

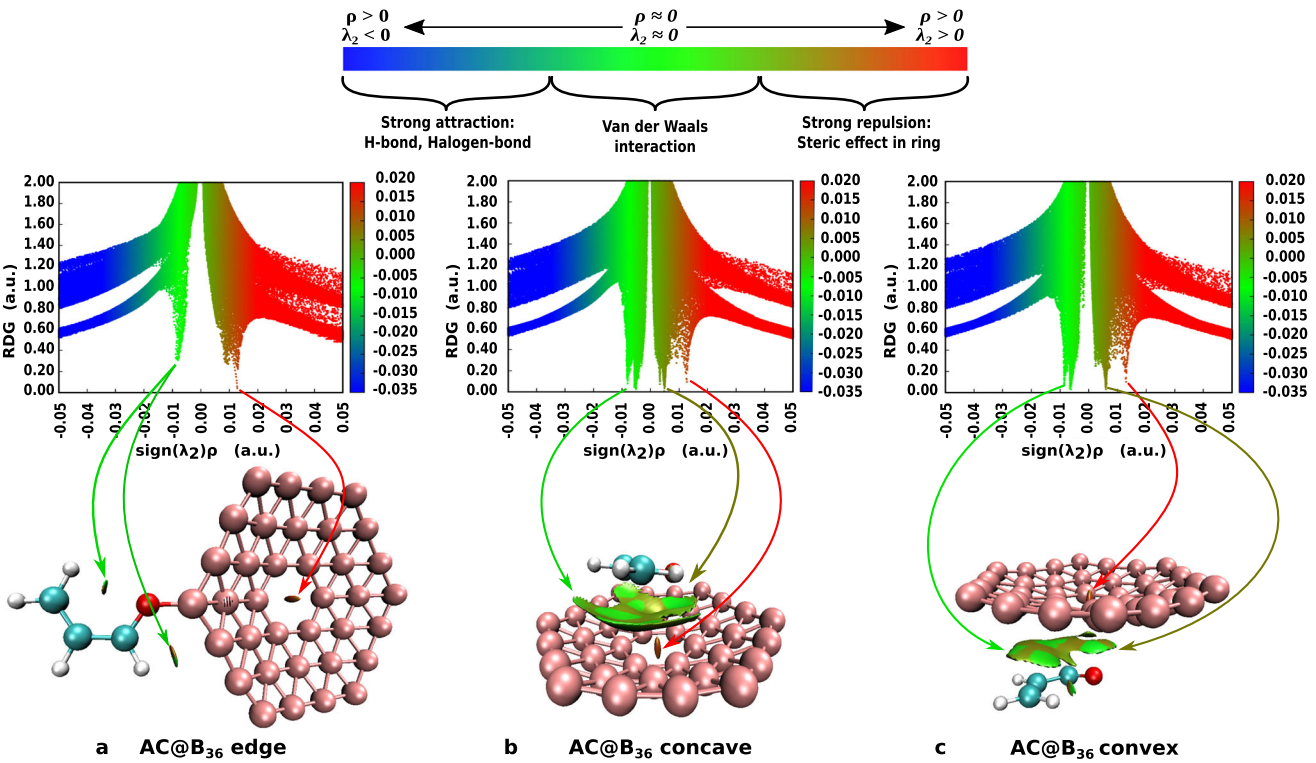

Fig. 6 The NCI-RDG isosurfaces (bottom) and scatter plot (upper) of (A) AC@B_{36} edge, (B) AC@B_{36} concave, and (C) AC@B_{36} convex

Table 3 Decomposed energy components (in kcal mol^{-1}) computed at the M06-2X/6-31G(d,p) level

Energy terms	AC@B_{36} concave	AC@B_{36} convex
Electrostatic	− 7.70	− 6.57
Exchange	− 10.16	− 9.66
Repulsion	+ 35.44	+ 30.08
Polarization	− 3.96	− 3.39
Dispersion	− 22.86	− 15.44
Total	− 9.24	− 4.97

$$s = \frac{1}{2(3\pi^2)^{1/3}} \frac{|\nabla\rho|}{\rho^{4/3}} \quad (3)$$

where ρ and $\nabla\rho$ are density and its first derivative, respectively. The regions and types of interactions between AC molecule and B_{36} nanosheet can be identified and visualized by colored RDG isosurface, in which the blue regions represent strong attractive interactions like H-bond, green denotes weak van der Waals interactions, and the red regions represent steric repulsion.

The RDG isosurfaces for the three complexes are shown in Fig. 6, with the color ranging from blue to red corresponding to the value of $-0.05 < \rho^*\text{sign}(\lambda 2) < 0.05$ a.u.

For AC@B_{36} concave and AC@B_{36} convex complexes, larger green isosurfaces (dark green and light green) were observed between AC molecule and B_{36} nanosheet, corresponding to the ranges between − 0.010 and − 0.015 a.u. (light green) and between − 0.01 a.u. and − 0.015 a.u. (dark green), which are characteristic of intermolecular van der Waals interactions, confirming that van der Waals (vdW) interactions are the key driving force for the adsorption of acrolein molecule on the B_{36} borophene in both AC@B_{36} concave and AC@B_{36} convex complexes.

In addition, for the AC@B_{36} edge complex, two green isosurfaces were determined. The first is located between hydrogen atom (H_{41}) of AC molecule and boron atom (B_{20}) of B_{36} borophene. The second isosurface is an intramolecular

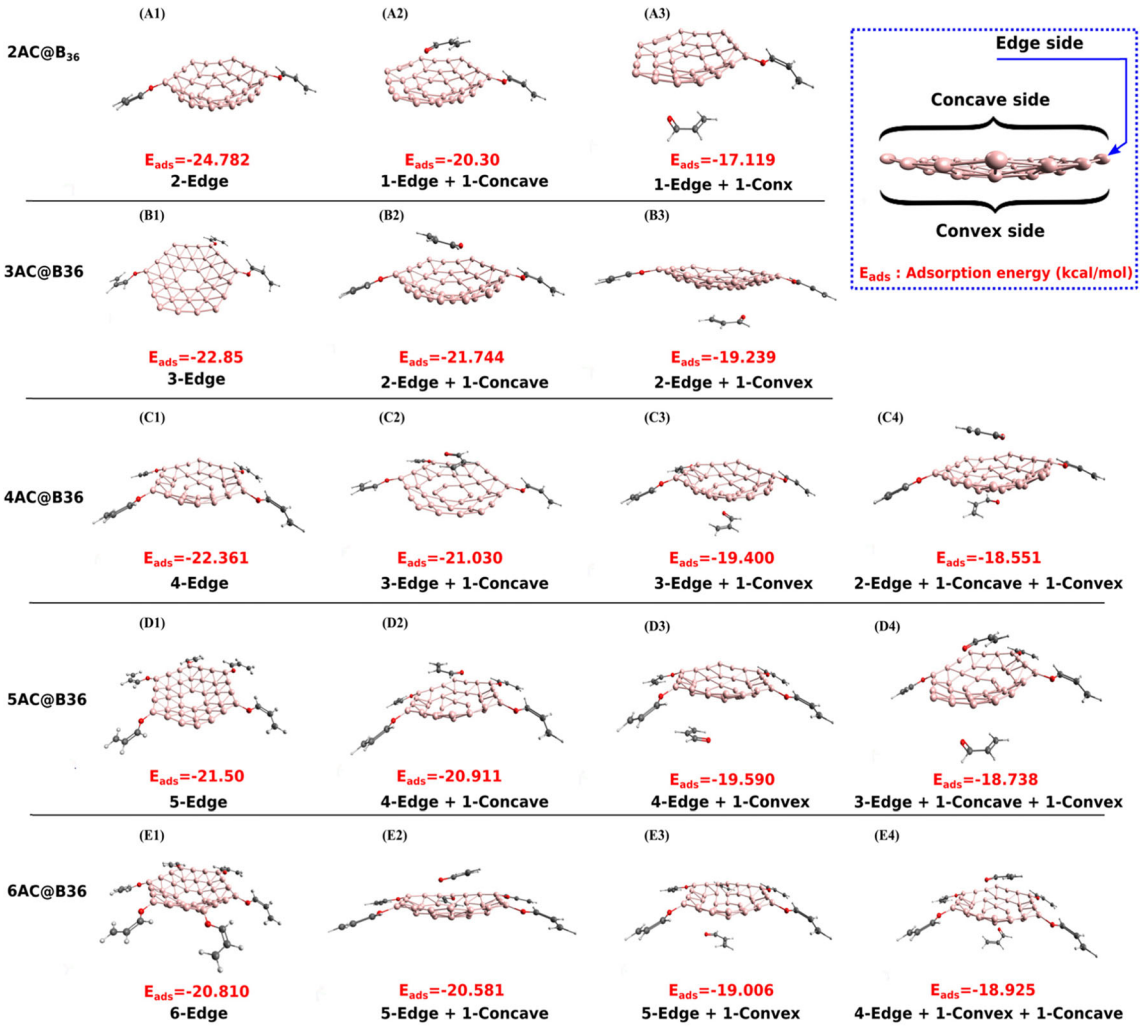

Fig. 7 Optimized geometry structures for studied complexes with multiple adsorbed AC molecules at B97-D3(BJ)/def2-SVP levels

Table 4 Adsorption energy (E_{ads}, kcal mol^{-1}), energy of HOMO and LUMO (E_{HOMO} and E_{LUMO}, eV), HOMO–LUMO energy gap ($|E_g|$, eV), and the percentage of variation of $|E_g|$ after the adsorption process ($|\Delta E_g|$) for studied complexes with multiple AC molecules at B97-D3(BJ)/def2-SVP computational levels

Complex	Configurations		E_{ads} (kcal mol^{-1})	E_{HOMO} (eV)	E_{LUMO} (eV)	$\|E_g\|$ (eV)	$\|\Delta E_g\|$ (%)
B_{36}			–	− 5.392	− 4.299	1.093	–
2AC@B_{36}	2-edge	(A1)	− 24.78	− 4.57	− 4.40	0.17	84.09
	1-edge + 1-concave	(A2)	− 20.30	− 4.90	− 4.55	0.35	67.80
	1-edge + 1-convex	(A3)	− 17.12	− 4.90	− 4.55	0.35	67.44
3AC@B_{36}	3-edge	(B1)	− 22.86	− 4.25	− 4.20	0.05	95.52
	2-edge + 1-concave	(B2)	− 21.75	− 4.53	− 4.36	0.17	84.27
	2-edge + 1-convex	(B3)	− 19.24	− 4.56	− 4.39	0.17	84.18
4AC@B_{36}	4-edge	(C1)	− 22.36	− 3.97	− 3.95	0.02	97.99
	3-edge + 1-concave	(C2)	− 21.03	− 4.24	− 4.14	0.10	91.77
	3-edge + 1-convex	(C3)	− 19.40	− 4.26	− 4.17	0.09	91.77
	2-edge + 1-concave + 1-convex	(C4)	− 18.55	− 4.51	− 4.34	0.17	84.54
5AC@B_{36}	5-edge	(D1)	− 21.50	− 3.88	− 3.86	0.02	98.17
	4-edge + 1-concave	(D2)	− 20.91	− 3.96	− 3.98	0.02	98.72
	4-edge + 1-convex	(D3)	− 19.59	− 3.99	− 4.01	0.02	98.45
	3-edge + 1-concave + 1-convex	(D4)	− 18.74	− 4.24	− 4.16	0.08	92.96
6AC@B_{36}	6-edge	(E1)	− 20.81	− 3.76	− 3.75	0.01	98.54
	5-edge + 1-concave	(E2)	− 20.58	− 3.84	− 3.82	0.02	98.35
	5-edge + 1-convex	(E3)	− 19.01	− 3.81	− 3.89	0.08	93.14
	4-edge + 1-concave + 1-convex	(E4)	− 18.93	− 3.98	− 4.00	0.02	98.17

interaction occurring between oxygen (O_{42}) of the carbonyl group and hydrogen atom (H_{44}) of AC molecule. These weak van der Waals interactions contribute to global stability and explain the orientation of AC molecule in the AC@B_{36} edge complex.

Energy decomposition analysis (EDA) was performed with GAMESS code for the analysis of intermolecular interactions between the acrolein and B_{36} borophene using M06-2X functional which is recommended for predicting and describing non-covalent interactions and 6-31G(d,p) basis set. The total interaction energy obtained from a complex calculation (AC@B_{36}) in both concave and convex configurations is decomposed into electrostatic, exchange, repulsion, and polarization terms; the computed decomposed energy terms are reported in Table 3.

From Table 3, it is clear that dispersive energy dominates the attractive energy components and provides the largest contribution to the total interaction energy, the dispersive energy of AC@B_{36} concave is greater by 7.42 kcal mol^{-1} than that of AC@B_{36} convex; however, the repulsion energy due to the destabilization is larger for AC@B_{36} concave (+ 35.44 kcal mol^{-1}) and higher than AC@B_{36} convex by 5.36 kcal mol^{-1}. These results are consistent with those obtained from the RDG-NCI analysis confirming that vdW dispersion interactions play a key role in the stabilization of both complexes.

Adsorption of multiple acrolein molecules on the B_{36} borophene

In order to examine the concentration effect on the adsorption of several acrolein molecules, we have investigated the adsorption of up to six acrolein molecules on the B_{36} surface. For this purpose, we firstly selected the most stable complex with a singly edge-adsorbed acrolein, and then, the additional acrolein molecules were added increasingly and successively at the edge, concave, and convex sides, while focusing primarily on the adsorption at the edge sides. A reoptimization procedure was performed for each configuration at B3LYP-D3(BJ)/def2-SVP, B97-D3(BJ)/def2-SVP, and M06-2X-D3(0)/def2-SVP computational levels. For each newly optimized complex, various possible configurations are compared as shown in Fig. 7. The calculated adsorption energy, energy of HOMO and LUMO, HOMO–LUMO gaps, and the percentage of variation of HOMO–LUMO gap $|\Delta E_g|$ for studied complexes with multiple AC molecules at the B97-D3(BJ)/def2-SVP theoretical level are reported in Table 4. Computational results obtained at B3LYP-D3(BJ)/def2-SVP and M06-2X-D3(0)/def2-SVP theoretical levels are listed in Tables S1 and S2 (see supplementary data).

From the calculated adsorption energies at the B97-D3(BJ)/def2-SVP level (Table 4), it is evident that the most

stable complexes are A1, B1, C1, D1, and E1, in which AC molecules are adsorbed at the edge sites of B_{36} nanosheet.

The results from Table 4 clearly show that the HOMO levels are shifted to upper energies whereas the LUMO levels are shifted to lower energies after the adsorption process, particularly when increasing the number of adsorbed AC molecules, leading to a significant decrease of the HOMO–LUMO energy gap. In addition, the percentage of variation of HOMO–LUMO gap $|\Delta E_g|$ exhibits greater values following the order: $2AC@_{36} < 3AC@_{36} < 4AC@_{36} < 5AC@b_{36} \approx 6AC@B_{36}$.

Based on these results, it can be concluded that the concentration of acrolein affects the electronic properties of borophene by decreasing the HOMO–LUMO gap and, therefore, increasing the electrical conductance. Thus, the borophene can serve as a sensing material for the detection of acrolein molecule.

Conclusions

Using DFT calculations, we extensively studied the electronic and geometrical properties of acrolein adsorption on B_{36} borophene nanosheet. Our results reveal that the B_{36} borophene bears a quasi-planar structure with a central hexagonal hole, and the neutral B_{36} nanosheet is more reactive than cationic and anionic species. The calculated values of the Fukui functions show that the most reactive sites are those located at the corner sites of neutral B_{36}, susceptible to both nucleophilic and electrophilic attacks; more specifically, the edge boron atoms are the most stable sites of adsorption. The acrolein molecule is attached to the borophene surface via the oxygen atom of its carbonyl group with an adsorption energy of − 25.20 kcal mol^{-1}. The NCI-RDG analysis highlighted the role of van der Waals interactions in stabilizing the adsorption of acrolein on both convex and concave surfaces of borophene, in accordance with the results of the energy decomposition analysis. Up to six acrolein molecules can be adsorbed preferentially at the edge sides of the B_{36} borophene. According to the calculated density of states, acrolein molecule affects strongly the electronic properties of B_{36} borophene by decreasing the HOMO–LUMO gap and, thus, inducing changes in its electrical conductance. B_{36} borophene nanosheet is expected to be applied as a nanosensor for detecting acrolein.

References

1. Zhang P, Wang F, Yu M, Zhuang X, Feng X (2018) Two-dimensional materials for miniaturized energy storage devices: from individual devices to smart integrated systems. Chem Soc Rev 47:7426–7451
2. Schwierz F, Pezoldt J, Granzner R (2015) Two-dimensional materials and their prospects in transistor electronics. Nanoscale 7: 8261–8283
3. Hynek DJ, Pondick JV, Cha JJ (2019) The development of 2D materials for electrochemical energy applications: a mechanistic approach. APL Mater 7:030902
4. Chhowalla M, Jena D, Zhang H (2016) Two-dimensional semiconductors for transistors. Nat Rev Mater 1:16052
5. Gupta A, Sakthivel T, Seal S (2015) Recent development in 2D materials beyond graphene. Prog Mater Sci 73:44–126
6. Wang Z, Mi B (2017) Environmental applications of 2D molybdenum disulfide (MoS_2) nanosheets. Environ Sci Technol 51: 8229–8244
7. Jun BM, Kim S, Heo J, Park CM, Her N, Jang M, Huang Y, Han J, Yoon Y (2019) Review of MXenes as new nanomaterials for energy storage/delivery and selected environmental applications. Nano Res 12:471–487
8. Kemp KC, Seema H, Saleh M, Le NH, Mahesh K, Chandra V, Kim KS (2013) Environmental applications using graphene composites: water remediation and gas adsorption. Nanoscale 5:3149–3171
9. Wang J, Ma F, Sun M (2017) Graphene, hexagonal boron nitride, and their heterostructures: properties and applications. RSC Adv 7:16801–16822
10. Kurapati R, Kostarelos K, Prato M, Bianco A (2016) Biomedical uses for 2D materials beyond graphene: current advances and challenges ahead. Adv Mater 28:6052–6074
11. Pradeep AV, Satya Prasad SV, Suryam LV, Prasanna Kumari P (2019) A review on 2D materials for bio-applications. Mater Today Proc 19:380–383
12. Novoselov KS, Geim AK, Morozov SV, Jiang D, Zhang Y, Dubonos SV, Grigorieva IV, Firsov AA (2004) Electric field effect in atomically thin carbon films. Science 306:666–669
13. Geim AK, Novoselov KS (2007) The rise of graphene. Nat Mater 6:183–191
14. Senese A, Chalifoux W (2019) Nanographene and graphene nanoribbon synthesis via alkyne benzannulations. Molecules 24: 118
15. Hosseinzadeh A, Bidmeshkipour S, Abdi Y, Arzi E, Mohajerzadeh S (2018) Graphene based strain sensors: a comparative study on graphene and its derivatives. Appl Surf Sci 448: 71–77
16. Calogero G, Alcón I, Papior N, Jauho AP, Brandbyge M (2019) Quantum interference engineering of nanoporous graphene for carbon nanocircuitry. J Am Chem Soc 141:13081–13088
17. Liao L, Peng H, Liu Z (2014) Chemistry makes graphene beyond graphene. J Am Chem Soc 136:12194–12200
18. Tao J, Tang H, Patra A, Bhattarai P, Perdew JP (2019) Erratum: Modeling the physisorption of graphene on metals. Phys Rev B 97 (2018) 165403. Phys Rev B Condens Matter Mater Phys 99: 169901
19. Tang Q, Zhou Z, Chen Z (2015) Innovation and discovery of graphene-like materials via density-functional theory computations: innovation and discovery of graphene-like materials via DFT computations. WIREs Comput Mol Sci 5:360–379
20. Rahali S, Belhocine Y, Touzeau J, Tangour B, Maurel F, Seydou M (2017) Balance between physical and chemical interactions of second-row diatomic molecules with graphene sheet. Superlattice Microst 102:45–55
21. Saxena S, Chaudhary RP, Shukla S (2016) Stanene: atomically thick free-standing layer of 2D hexagonal tin. Sci Rep 6:31073
22. Gao J, Zhang G, Zhang YW (2016) Exploring Ag(111) substrate for epitaxially growing monolayer stanene: a first-principles study. Sci Rep 6:29107

23. Zhu F, Chen W, Xu Y, Gao C, Guan D, Liu C, Qian D, Zhang SC, Jia JF (2015) Epitaxial growth of two-dimensional stanene. Nat Mater 14:1020–1025
24. Yuhara J, Fujii Y, Nishino K, Isobe N, Nakatake M, Xian L, Rubio A, Le Lay G (2018) Large area planar stanene epitaxially grown on Ag(111). 2D Mater 5:025002
25. Dávila ME, Xian L, Cahangirov S, Rubio A, Le Lay G (2014) Germanene: a novel two-dimensional germanium allotrope akin to graphene and silicene. New J Phys 16:095002
26. Reis F, Li G, Dudy L, Bauernfeind M, Glass S, Hanke W, Thomale R, Schäfer J, Claessen R (2017) Bismuthene on a SiC substrate: a candidate for a high-temperature quantum spin Hall material. Science 357:287–290
27. Mannix AJ, Zhou XF, Kiraly B, Wood JD, Alducin D, Myers BD, Liu X, Fisher BL, Santiago U, Guest JR, Yacaman MJ, Ponce A, Oganov AR, Hersam MC, Guisinger NP (2015) Synthesis of borophenes: anisotropic, two-dimensional boron polymorphs. Science 350:1513–1516
28. Feng B, Zhang J, Zhong Q, Li W, Li S, Li H, Cheng P, Meng S, Chen L, Wu K (2016) Experimental realization of two-dimensional boron sheets. Nat Chem 8:563–568
29. Tai G, Hu T, Zhou Y, Wang X, Kong J, Zeng T, You Y, Wang Q (2015) Synthesis of atomically thin boron films on copper foils. Angew Chem Int Ed 54:15473–15477
30. Zhang Z, Yang Y, Gao G, Yakobson BI (2015) Two-dimensional boron monolayers mediated by metal substrates. Angew Chem Int Ed 54:13022–13026
31. Wu X, Dai J, Zhao Y, Zhuo Z, Yang J, Zeng XC (2012) Two-dimensional boron monolayer sheets. ACS Nano 6:7443–7453
32. Liu X, Zhang Z, Wang L, Yakobson BI, Hersam MC (2018) Intermixing and periodic self-assembly of borophene line defects. Nat Mater 17:783–788
33. Boustani I (1997) Systematic ab initio investigation of bare boron clusters: determination of the geometry and electronic structures of B_n (n=2–14). Phys Rev B 55:16426
34. Li WL, Chen X, Jian T, Chen TT, Li J, Wang LS (2017) From planar boron clusters to borophenes and metalloborophenes. Nat Rev Chem 1:0071
35. Luo XM, Jian T, Cheng LJ, Li WL, Chen Q, Li R, Zhai HJ, Li SD, Boldyrev AI, Li J, Wang LS (2017) B_{26}^-: the smallest planar boron cluster with a hexagonal vacancy and a complicated potential landscape. Chem Phys Lett 683:336–341
36. Zhao J, Wang L, Li F, Chen Z (2010) B_{80} and other medium-sized boron clusters: core-shell structures, not hollow cages. J Phys Chem A 114:9969–9972
37. Jian T, Chen X, Li SD, Boldyrev AI, Li J, Wang LS (2019) Probing the structures and bonding of size-selected boron and doped-boron clusters. Chem Soc Rev 48:3550–3591
38. Piazza ZA, Hu HS, Li WL, Zhao YF, Li J, Wang LS (2014) Planar hexagonal B_{36} as a potential basis for extended single-atom layer boron sheets. Nat Commun 5:3113
39. Tang H, Ismail-Beigi S (2007) Novel precursors for boron nanotubes: the competition of two-center and three-center bonding in boron sheets. Phys Rev Lett 99:115501
40. Yang X, Ding Y, Ni J (2008) Ab initio prediction of stable boron sheets and boron nanotubes: structure, stability, and electronic properties. Phys Rev B 77:041402
41. Penev ES, Bhowmick S, Sadrzadeh A, Yakobson BI (2012) Polymorphism of two-dimensional boron. Nano Lett 12:2441–2445
42. Er S, de Wijs GA, Brocks G (2009) DFT study of planar boron sheets: a new template for hydrogen storage. J Phys Chem C 113: 18962–18967
43. Zhang Z, Penev ES, Yakobson BI (2017) Two-dimensional boron: structures, properties and applications. Chem Soc Rev 46:6746–6763
44. Wang ZQ, Lü TY, Wang HQ, Feng YP, Zheng JC (2019) Review of borophene and its potential applications. Front Phys 14:33403
45. Jiang HR, Lu Z, Wu MC, Ciucci F, Zhao TS (2016) Borophene: a promising anode material offering high specific capacity and high rate capability for lithium-ion batteries. Nano Energy 23:97–104
46. Zhang X, Hu J, Cheng Y, Yang HY, Yao Y, Yang SA (2016) Borophene as an extremely high capacity electrode material for Li-ion and Na-ion batteries. Nanoscale 8:15340–15347
47. Shukla V, Wärnå J, Jena NK, Grigoriev A, Ahuja R (2017) Toward the realization of 2D borophene based gas sensor. J Phys Chem C 121:26869–26876
48. Omidvar A (2017) Borophene: a novel boron sheet with a hexagonal vacancy offering high sensitivity for hydrogen cyanide detection. Comput Theor Chem 1115:179–184
49. Yeager RP, Kushman M, Chemerynski S, Weil R, Fu X, White M, Callahan-Lyon P, Rosenfeldt H (2016) Proposed mode of action for acrolein respiratory toxicity associated with inhaled tobacco smoke. Toxicol Sci 151:347–364
50. Feng Z, Hu W, Hu Y, Tang MS (2006) Acrolein is a major cigarette-related lung cancer agent: preferential binding at p53 mutational hotspots and inhibition of DNA repair. Proc Natl Acad Sci 103:15404–15409
51. Rastegar SF, Hadipour NL, Tabar MB, Soleymanabadi H (2013) DFT studies of acrolein molecule adsorption on pristine and Al-doped graphenes. J Mol Model 19:3733–3740
52. Karami AR (2015) Acrolein adsorption on graphyne nanotube: a density functional theory study. Fuller Nanotub Car N 23:885–889
53. Dheivamalar S, Banu KB (2019) A DFT study on functionalization of acrolein on Ni-doped $(ZnO)_6$ nanocluster in dye-sensitized solar cells. Heliyon 5:e02903
54. Abbasi A, Sardroodi JJ (2016) The interaction of acrolein with pristine and N-doped TiO_2 anatase nanoparticles: a DFT study. Acta Chim Slov 63:713–720
55. Pirillo S, López-Corral I, Germán E, Juan A (2014) Density functional study of acrolein adsorption on Pt(111). Vacuum 99:259–264
56. Loffreda D, Jugnet Y, Delbecq F, Bertolini JC, Sautet P (2004) Coverage dependent adsorption of acrolein on Pt(111) from a combination of first principle theory and HREELS study. J Phys Chem B 108:9085–9093
57. Kang GJ, Chen ZX, Li Z (2011) Acrolein adsorption on gold clusters, a theoretical study of conjugation effect on C=C and C=O interaction with Au clusters. Catal Lett 141:996–1003
58. Ferullo R, Branda MM, Illas F (2010) Coverage dependence of the structure of acrolein adsorbed on Ag(111). J Phys Chem Lett 1: 2546–2549
59. Grimme S, Antony J, Ehrlich S, Krieg H (2010) A consistent and accurate ab initio parametrization of density functional dispersion correction (DFT-D) for the 94 elements H-Pu. J Chem Phys 132: 154104
60. Grimme S, Ehrlich S, Goerigk L (2011) Effect of the damping function in dispersion corrected density functional theory. J Comput Chem 32:1456–1465
61. Johnson ER, Becke AD (2006) A post-Hartree-Fock model of intermolecular interactions: inclusion of higher-order corrections. J Chem Phys 124:174104
62. Becke AD, Johnson ER (2005) A density-functional model of the dispersion interaction. J Chem Phys 123:154101
63. Becke AD (1997) Density-functional thermochemistry. V. Systematic optimization of exchange-correlation functionals. J Chem Phys 107:8554–8560
64. Zhao Y, Truhlar DG (2008) The M06 suite of density functionals for main group thermochemistry, thermochemical kinetics, noncovalent interactions, excited states, and transition elements: two new functionals and systematic testing of four M06-class

functionals and 12 other functionals. Theor Chem Accounts 120: 215–241
65. Schäfer A, Horn H, Ahlrichs R (1992) Fully optimized contracted Gaussian basis sets for atoms Li to Kr. J Chem Phys 97:2571–2577
66. Schäfer A, Huber C, Ahlrichs R (1994) Fully optimized contracted Gaussian basis sets of triple zeta valence quality for atoms Li to Kr. J Chem Phys 100:5829–5835
67. Weigend F (2006) Accurate Coulomb-fitting basis sets for H to Rn. Phys Chem Chem Phys 8:1057–1065
68. Neese F (2018) Software update: the ORCA program system. Version 4.0: software update. Wiley Interdiscip Rev Comput Mol Sci 8:e1327
69. Neese F, Wennmohs F, Hansen A, Becker U (2009) Efficient, approximate and parallel Hartree–Fock and hybrid DFT calculations. A 'chain-of-spheres' algorithm for the Hartree–Fock exchange. Chem Phys 356:98–109
70. Neese F (2003) An improvement of the resolution of the identity approximation for the formation of the Coulomb matrix. J Comput Chem 24:1740–1747
71. Eichkorn K, Treutler O, Öhm H, Häser M, Ahlrichs R (1995) Auxiliary basis sets to approximate Coulomb potentials. Chem Phys Lett 240:283–290
72. Kruse H, Grimme S (2012) A geometrical correction for the inter- and intra-molecular basis set superposition error in Hartree-Fock and density functional theory calculations for large systems. J Chem Phys 136:154101
73. Hanwell MD, Curtis DE, Lonie DC, Vandermeersch T, Zurek E, Hutchison GR (2012) Avogadro: an advanced semantic chemical editor, visualization, and analysis platform. J Cheminf 4:17
74. Johnson ER, Keinan S, Mori-Sánchez P, Contreras-García J, Cohen AJ, Yang W (2010) Revealing noncovalent interactions. J Am Chem Soc 132:6498–6506
75. Lu T, Chen F (2012) Multiwfn: a multifunctional wavefunction analyzer. J Comput Chem 33:580–592
76. Humphrey W, Dalke A, Schulten K (1996) VMD: visual molecular dynamics. J Mol Graph 14:33–38
77. Schmidt MW, Baldridge KK, Boatz JA, Elbert ST, Gordon MS, Jensen JH, Koseki S, Matsunaga N, Nguyen KA, Su S, Windus TL, Dupuis M, Montgomery JA (1993) General atomic and molecular electronic structure system. J Comput Chem 14:1347–1363
78. Hariharan PC, Pople JA (1973) The influence of polarization functions on molecular orbital hydrogenation energies. Theor Chim Acta 28:213–222
79. Valadbeigi Y, Farrokhpour H, Tabrizchi M (2015) Adsorption of small gas molecules on B_{36} nanocluster. J Chem Sci 127:2029–2038
80. Rostami Z, Soleymanabadi H (2016) N–H bond cleavage of ammonia on graphene-like B_{36} borophene: DFT studies. J Mol Model 22:70
81. Rastgou A, Soleymanabadi H, Bodaghi A (2017) DNA sequencing by borophene nanosheet via an electronic response: a theoretical study. Microelectron Eng 169:9–15
82. Shahbazi Kootenaei A, Ansari G (2016) B_{36} borophene as an electronic sensor for formaldehyde: quantum chemical analysis. Phys Lett A 380:2664–2668
83. Solimannejad M, Kamalinahad S, Shakerzadeh E (2017) $Li_n@B_{36}$ (n = 1, 2) nanosheet with remarkable electro-optical properties: a DFT study. J Electron Mater 46:4420–4425
84. Mohsenpour Z, Shakerzadeh E, Zare M (2017) Quantum chemical description of formaldehyde (HCHO), acetaldehyde (CH_3CHO) and propanal (CH_3CH_2CHO) pollutants adsorption behaviors onto the bowl-shaped B_{36} nanosheet. Adsorption 23:1041–1053
85. Shahsavar A, Mohajeri A (2018) Impact of position and number of nitrogen atom substitution on the curvature and hydrogen adsorption properties of metallized borophene. J Mater Sci 53:4540–4553
86. Li WY, Zhao X, Dang JS (2019) A mechanistic study of B_{36}-supported atomic au promoted CO_2 electroreduction to formic acid. J Mater Chem A 7:13935–13940
87. Hassani A, Mosavian MTH, Ahmadpour A, Farhadian N (2016) A comparative theoretical study of methane adsorption on the nitrogen, boron and lithium doped graphene sheets including density functional dispersion correction. Comput Theor Chem 1084: 43–50
88. Hosseinian A, Asadi Z, Edjlali L, Bekhradnia A, Vessally E (2017) NO_2 sensing properties of a borazine doped nanographene: a DFT study. Comput Theor Chem 1106:36–42
89. Montejo-Alvaro F, Oliva J, Herrera-Trejo M, Hdz-García HM, Mtz-Enriquez AI (2019) DFT study of small gas molecules adsorbed on undoped and N-, Si-, B-, and Al-doped graphene quantum dots. Theor Chem Accounts 138:37
90. Jin P, Hou Q, Tang C, Chen Z (2015) Computational investigation on the endohedral borofullerenes $M@B_{40}$ (M=Sc, Y, La). Theor Chem Accounts 134:1–10
91. Allal H, Belhocine Y, Zouaoui E (2018) Computational study of some thiophene derivatives as aluminium corrosion inhibitors. J Mol Liq 265:668–678
92. Ammouchi N, Allal H, Belhocine Y, Bettaz S, Zouaoui E (2020) DFT computations and molecular dynamics investigations on conformers of some pyrazinamide derivatives as corrosion inhibitors for aluminum. J Mol Liq 300:112309
93. Sánchez-Márquez J (2019) New advances in conceptual-DFT: an alternative way to calculate the Fukui function and dual descriptor. J Mol Model 25:123
94. Wu J, Yan H, Zhong A, Chen H, Jin Y, Dai G (2019) Theoretical and conceptual DFT study of pnicogen- and halogen-bonded complexes of PH_2X—BrCl. J Mol Model 25:28
95. Vessally E, Soleimani-Amiri S, Hosseinian A, Edjlali L, Bekhradnia A (2017) The Hartree-Fock exchange effect on the CO adsorption by the boron nitride nanocage. Phys E 87:308–311
96. De H, Paul A, Datta A (2017) Theoretical study of Au_4 thymine, Au_{20} and Ag_{20} uracil and thymine complexes for surface enhanced Raman scattering. Comput Theor Chem 1111:1–13
97. Pahlavan F, Hosseinnezhad S, Samieadel A, Hung A, Fini E (2019) Fused aromatics to restore molecular packing of aged bituminous materials. Ind Eng Chem Res 58:11939–11953
98. Ni Y, Pan Y, Zhang J, Gu X, Pan X, Jiang J, Wang Q (2018) Theoretical study on reaction mechanism of thermal decomposition of dialkyl peroxides. Comput Theor Chem 1135:11–17
99. Zhang L, Wang JM, Wang QR, Zhang DW, Li ZT, Li ZM (2015) Theoretical investigation on SnCl4-catalyzed tandem dimerization/oxy-2-azonia-Cope rearrangements between β,γ-unsaturated ketones and imines. Theor Chem Accounts 134:4
100. Liang Z, Wang H, Zheng X, Wang X (2020) Theoretical investigation on rotaxanes containing a pyridyl-acyl hydrazone moiety: chemical Z → E and photochemical E → Z isomerizations. Theor Chem Accounts 139:39